

A Three-Dimensional Perspective on Extratropical Cyclone Impacts

ACACIA PEPLER AND ANDREW DOWDY

Australian Bureau of Meteorology, Melbourne, Victoria, Australia

(Manuscript received 20 June 2019, in final form 13 January 2020)

ABSTRACT

Cyclones can be identified from gridded pressure data at different levels of the troposphere, with vertical structure known to influence the temporal development and impacts of midlatitude cyclones. However, studies of midlatitude cyclones typically focus on cyclones identified at a single atmospheric level. This paper examines how the frequency of vertically organized or deep cyclones varies around the world, with a focus on southeastern Australia. About 50% of global cyclones identified from mean sea level pressure show a coherent vertical structure extending to at least 500 hPa, based on ERA-Interim reanalysis data, and shallow cyclones are most common in the global midlatitudes. Using a combination of reanalysis data and satellite-based rainfall and lightning, we show that in southeast Australia deep cyclones have higher intensities, longer durations, and more severe winds and rainfall than either shallow surface cyclones or upper-level cyclones with no surface low, motivating a three-dimensional approach for future cyclone analyses.

1. Introduction


Intense low pressure systems are a common occurrence in the global midlatitudes and extratropics, where they can cause severe weather including heavy rainfall, strong winds, and large waves (Leckebusch and Ulbrich 2004; Pfahl and Wernli 2012; Dowdy and Catto 2017). In southeastern Australia, the midlatitude cyclones locally known as east coast lows (Dowdy et al. 2019) have been shown to cause the majority of coastal floods (Callaghan and Power 2014), large waves (Dowdy et al. 2014), and shipwrecks (Callaghan and Helman 2008), as well as being critically important for rainfall variability and dam inflows (Pepler and Rakich 2010).

Owing to their significant impacts, as well as their important role in the poleward transport of heat and momentum (Chang et al. 2002), extratropical cyclones have been broadly researched across the globe. The majority of studies identify cyclones based on a closed circulation or vorticity maxima close to the surface, typically from gridded fields of sea level pressure or 850-hPa geopotential height from one or more reanalyses

and using one of several automated tracking methods (e.g., Hoskins and Hodges 2002; Wernli and Schwerz 2006; Murray and Simmonds 1991). Strong and long-lived cyclones tend to be consistently identified, but choices of tracking method, data source, and resolution can have a large influence on the detection of weaker systems (Neu et al. 2013; Pepler et al. 2015; Di Luca et al. 2015).

While cyclones are typically identified from surface fields, the vertical structure of a cyclone is known to play a major role in its development and impacts. Midtropospheric fields are frequently used to classify cyclones into subtypes, including by segregating into warm-core, cold-core, and hybrid systems (Hart 2003; Evans and Boyer-Souchet 2012; Yanase et al. 2014; Cavicchia et al. 2019; Quinting et al. 2019) and by using clustering approaches (Catto 2018; Graf et al. 2017). Case studies of severe and impactful cyclones in multiple regions have shown that these are typically associated with strong cyclonic vorticity near 500 hPa, often with a strong upper trough or cutoff low (Mills et al. 2010; Flaounas et al. 2015). This has led to 500-hPa geostrophic vorticity being applied as an indicator of likely surface cyclogenesis and associated severe weather conditions for model evaluations and climate projections, in part due to the larger spatial scale of upper cyclones (Dowdy et al. 2013b, 2014).

Compared to surface cyclones, fewer studies have explicitly identified and tracked cyclones at upper levels

 Denotes content that is immediately available upon publication as open access.

Corresponding author: Acacia Pepler, acacia.pepler@bom.gov.au

of the atmosphere, despite the importance of upper cyclonicity for surface cyclone development (Keable et al. 2002; Fuenzalida et al. 2005; Lim and Simmonds 2007). The University of Melbourne cyclone tracking scheme applied in this paper has previously been used for vertical tracking in the Southern Hemisphere (Lim and Simmonds 2007) and for explosive cyclones in the Mediterranean (Kouroutzoglou et al. 2012, 2015). For the Southern Hemisphere, Lim and Simmonds (2007) showed that cyclones are most common at the surface and at 500 hPa, with a minimum in cyclone frequency at 700 hPa, and that 52% of Southern Hemisphere cyclones can be considered “vertically well organized,” extending from the surface up to 500 hPa. However, while they identified the vertically well-organized cyclones as typically larger, more intense, and longer-lived than shallower cyclones, any differences between vertically organized and shallow cyclones in surface impacts remain unclear. More recently, Lakkis et al. (2019) have developed a more complex 4D cyclone tracking scheme based on the methods of Hoskins and Hodges (2005), which was applied over the Southern Hemisphere for the season June–August 2015.

In this study, we first build on the results of Lim and Simmonds (2007) for the Southern Hemisphere to show the global distribution of cyclones at various vertical levels, and how the relative frequency of vertical organization varies across the globe. In sections 5 and 6 we then focus on southeastern Australia, where both surface and 500-hPa fields have been used when analyzing cyclone frequency, to quantify the role of cyclone vertical structure on the impacts of cyclones near the surface, including how the vertical structure and impacts of a cyclone develop over time. The results highlight the potential benefits of using multiple atmospheric levels for tracking and analysis of cyclones.

2. Methods and data

Cyclones are identified using 6-hourly 0.75° resolution gridded mean sea level pressure (MSLP) and the 925-, 850-, 700-, 600-, 500-, 300-, and 200-hPa geopotential height (GPH) fields from the ERA-Interim reanalysis (Dee et al. 2011; ECMWF 2009). This is one of the most widely used reanalyses, and was chosen due to its high resolution and good skill at representing global climate including cyclones and other synoptic systems (Wang et al. 2006; Tilinina et al. 2013; Rudeva and Simmonds 2015). For some results analyses are shown for two half-years May–October (MJJASO) and November–April (NDJFMA) to capture the distinct seasonal patterns in each hemisphere.

There are a large number of cyclone tracking schemes available, with general agreement between methods for

strong cyclones and higher uncertainty for weaker and shallower systems (Neu et al. 2013; Pepler et al. 2015). While each method has advantages and disadvantages, for this paper we use the well-established University of Melbourne cyclone tracking scheme (Murray and Simmonds 1991; Simmonds et al. 1999; Simmonds and Keay 2000). This method has been widely used for studies of cyclone behavior across the globe (Jones and Simmonds 1993; Pezza and Ambrizzi 2003; Allen et al. 2010; Grieger et al. 2014; Pinto et al. 2005; Mesquita et al. 2009; Simmonds and Rudeva 2014), including studies of the vertical structure of cyclones with altitude (Lim and Simmonds 2007; Kouroutzoglou et al. 2012, 2015).

The cyclone tracking scheme can be applied to any gridded field, including MSLP and GPH at different pressure levels. The tracking scheme first bilinearly regrids this data onto a polar stereographic grid for each hemisphere, with the grid in this study chosen to give an effective resolution of 0.5° . Diffusive smoothing is also applied with a radius of 0.5° to minimize the influence of erroneous gridscale lows that can be common in some reanalyses (Pepler et al. 2018). Cyclones are first identified as maxima in the Laplacian of the field, with an iterative technique then employed to identify a corresponding pressure minimum from a spline-fitted pressure field, which can be either a closed or open circulation. Cyclones are then filtered based on the average Laplacian within a 2° radius, with additional filtering of cyclones identified from MSLP data to remove erroneous lows in the presence of topography above 1000 m. Finally, cyclones are grouped into events using a probability matching function.

For this paper, cyclones were initially required to exceed a minimum Laplacian of $10 \text{ m (degrees latitude)}^{-2}$, which is equivalent to 1.2 hPa (degrees latitude) $^{-2}$ at sea level using the hydrostatic equation. Both closed and open cyclones are included in the analysis, noting that strong upper-level geostrophic vorticity has been used as a diagnostic of both open and closed lows in eastern Australia (Dowdy et al. 2011, 2014). Additionally, distinguishing closed from open systems can be sensitive to data source, although results presented in this study were checked and found to be broadly similar when restricted to closed cyclones only. For completeness, we present results for cyclones across the globe, rather than arbitrarily selecting a latitude at which to stop tracking. However, it is important to note that the tracking method has been optimized for cyclones that occur outside the tropics and that the occurrence of cyclones in the tropics may be underestimated, particularly those tropical cyclones with relatively small radii.

In addition to the constant threshold, for sections 4–6 we applied height-varying intensity thresholds based on

TABLE 1. Height-varying intensity thresholds (m) used for vertically tracking cyclones in the ECL region (25°–40°S, 148°–160°E) and their average frequency of occurrence, shown for the six pressure levels used in this study.

	MSLP	925 hPa	850 hPa	700 hPa	600 hPa	500 hPa	300 hPa	200 hPa
Threshold (m)	12 (1.4 hPa)	12	10.5	10	13	18.5	23.5	55
Events per year	28.6	27.0	27.6	26.8	27.6	27.8	26.2	31.5
Hours per year	79.1	83.1	88.1	83.3	80.2	74.4	36.8	37.0
Days per year	36.9	36.1	37.5	37.5	38.4	36.6	74.9	64.0

the average Laplacian within a 2° radius of the cyclone center (Table 1) to give a constant number of east coast lows (ECLs) in the region 25°–40°S, 148°–160°E at each level, as the frequency of cyclones for a constant threshold is lowest at middle levels of the atmosphere (Lim and Simmonds 2007). No minimum duration thresholds are required, in order to avoid unnecessarily breaking the vertical tracking of cyclones in cases where cyclone tracks are inappropriately broken in time, such as due to merging and splitting of cyclone tracks, which can affect up to 20% of cyclones using an older version of this tracking method (Pepler and Coutts-Smith 2013).

Vertical tracking in this paper follows the approach used in Lim and Simmonds (2007), but cyclones are both tracked upward from the surface and downward from the 500-hPa level. Vertical tracking is performed for each instance of a cyclone rather than just at the moment of maximum intensity. For each cyclone identified at the surface (or 500 hPa), we search for a corresponding cyclone within a 500-km radius at the next vertical level. If a “partner” cyclone was found, the subsequent level is then searched for a cyclone within a 500-km radius of the partner cyclone. This is continued until there is no partner cyclone identified at a given level. While surface cyclones are traced to as high as 200 hPa, upper-level cyclones are only traced downward from 500 hPa, as 500 hPa has been previously used as a level for identifying upper-level cyclones that may have surface impacts (Dowdy et al. 2014; Pook et al. 2014). This vertical tracking is illustrated in Fig. 1. The choice of a constant 500-km radius is somewhat arbitrary, similar to the constant radius of 444 km used in Lim and Simmonds (2007). While a variable radius that accounts for the different height differences between levels was tested as per Kouroutzoglou et al. (2012), it made little difference to results.

Throughout this paper we will discuss five subcategories of cyclones, indicated in Fig. 1. Similar to Lim and Simmonds (2007), analysis in this paper will focus on the subsets of “surface” cyclones including “shallow surface cyclones” (below 850 hPa) and “deep surface cyclones” (MSLP > 500 hPa), although some results will also be presented for cyclones of intermediate depth (“midlevel cyclones”) where a surface low is tracked to 700 or

600 hPa but does not have a corresponding 500-hPa “upper” cyclone. In addition, we will show results for “shallow upper cyclones,” which are identified at 500 hPa but have no surface low (i.e., the lowest level is 700 hPa or higher), and “deep upper cyclones” (500 hPa → MSLP).

Analysis is performed both on individual cyclone instances and using an event-based framework that accounts for the vertical development of cyclones over time, with events classified as shallow or deep based on their deepest instance (i.e., a surface cyclone that is tracked to 500 hPa at any point during its lifetime is considered a deep surface cyclone).

For each cyclone, the automated cyclone tracking scheme also records the central pressure/height, the average Laplacian within a 2° radius of the center, the effective radius of the cyclone, and the depth (in hPa or m) between the cyclone center and the average field at the edge of the cyclone, as described in Simmonds and Keay (2000). Cyclones near the east coast of Australia are also classified into warm core, cold core, or hybrid systems as per the Hart (2003) phase space using data from Cavicchia et al. (2019), with events grouped based on the dominant phase space category across times within the region of interest.

Several cyclone-centered fields are obtained for a 10° radius around each cyclone within the Australian region, with the average and maximum of the field over a 5° radius from the cyclone center calculated as an indicator of the cyclone impacts. From ERA-Interim, we obtain the MSLP and 500-hPa GPH, the zonal and meridional components of the 10-m wind (U10/V10) as well as the scalar wind speed (WS), and the total column water (TCW). To help examine the environmental conditions associated with ECLs, we also calculate the 700-hPa Brunt–Väisälä frequency (BV700) and convective available potential energy (CAPE) as measures of atmospheric stability. We use the “most unstable” CAPE, which is calculated using the most unstable level based on maximum equivalent potential temperature. To supplement the ERA-Interim fields, instantaneous rain rates were also obtained from the Tropical Rainfall Measuring Mission (TRMM) multisatellite precipitation analysis 3B42 V7 (Huffman et al. 2007; TRMM 2011) at a

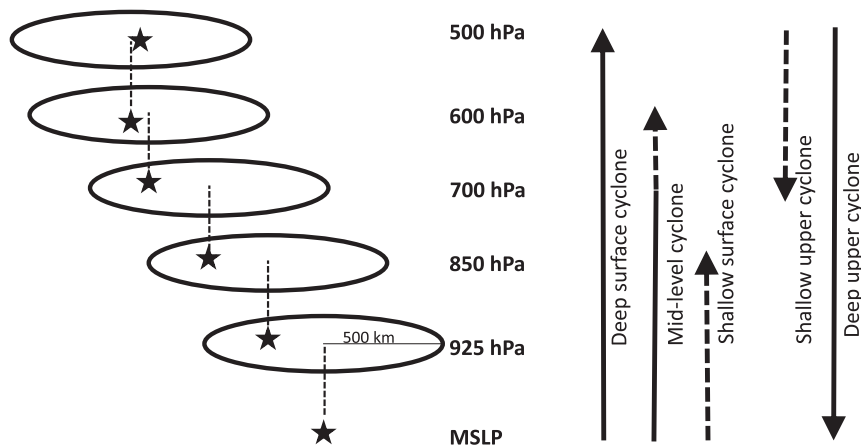


FIG. 1. Schematic showing the vertical tracking process and the levels included for each subcategory of cyclone. Stars indicate the location of a low at each level, relative to the 500-km searching radius. On the right, lines are solid for levels to which the cyclone must be tracked, and dashed for optional levels where cyclones that fail to reach that level are still incorporated in the category. For example, a midlevel cyclone must be tracked from the surface to at least 700 hPa, and cyclones that reach 600 hPa are also included in the category.

0.25° resolution between 1998 and 2015, which was available for 99% of surface ECLs during this period. Additionally, lightning stroke counts within ± 3 h of the observation time were obtained from the World Weather Lightning Network (WWLN; Hutchins et al. 2013; Virts et al. 2013) between 2005 and 2015, noting that a single lightning flash as perceived from a human eye can sometimes contain multiple lightning strokes (known as flash “multiplicity”).

3. Cyclone climatology with height

a. Broad-scale features for individual levels

Figure 2 shows the average number of cyclones identified per year across the globe for each vertical level, using a constant intensity threshold with height of $1.2 \text{ m (degrees latitude)}^{-2}$. Globally, cyclones are most common in the main midlatitude storm tracks, particularly at the surface and 500 hPa, with lowest occurrence

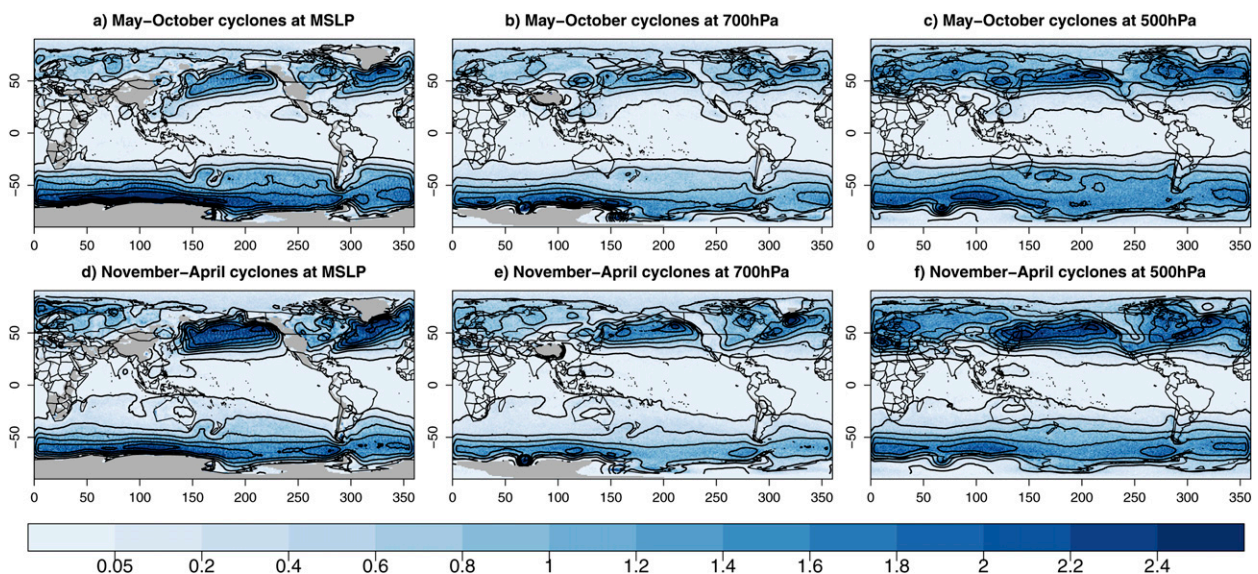


FIG. 2. Average frequency of cyclones [centers (degrees latitude) $^{-2}$] in ERA-Interim between 1979 and 2016 at different vertical levels during (top) May–October and (bottom) November–April. Solid contours show frequencies of 0.05 centers (degrees latitude) $^{-2}$ and then every 0.5 using a 5° averaging window.

TABLE 2. Selected statistics for global cyclones identified at different vertical levels. Note that the MSLP cyclone tracking excluded any cyclones identified at elevations above 1000 m.

	MSLP	925 hPa	850 hPa	700 hPa	600 hPa	500 hPa	300 hPa	200 hPa
Events per year	15 107	18 179	13 348	9465	10 516	13 142	17 511	6553
Average duration (h)	24.1	20.8	22.5	26.4	28.0	30.5	26.9	14.5
Total instances per year	60 377	81 196	63 505	51 140	59 486	80 000	95 860	19 972
Average Laplacian [hPa (degrees latitude) ⁻²]	17.7	16.7	16.7	16.5	16.8	18.3	19.0	84.4
Average radius (degrees)	3.2	2.9	3.2	3.7	3.9	3.8	3.9	8.9
Average velocity (km h ⁻¹)	44.2	35.9	35.5	34.5	37.2	40.4	39.6	33.6
% of instances with closed circulation	65%	67%	69%	69%	61%	52%	45%	47%
% May–October (SH)	57%	57%	57%	57%	57%	56%	52%	44%
% November–April (NH)	59%	51%	52%	54%	55%	55%	45%	28%

frequencies observed at 700 hPa, consistent with Lim and Simmonds (2007). At all levels, cyclones are most common during the cool half of the year in both hemispheres, noting that this tracking scheme is not designed for tropical cyclones and is run on a polar stereographic grid and so may underestimate cyclone frequencies in the tropics.

Globally, cyclones tend to have larger radii and longer durations when identified at higher altitudes than lower altitudes (Table 2), noting that data for MSLP cyclones exclude all cyclones identified at elevations above 1000 m. Cyclones identified at 700 hPa have the lowest average intensities and movement speeds and are the most likely to have closed circulations, whereas at 500 hPa close to half of all identified cyclones have open circulation. Cyclones identified at 200 hPa have very different characteristics from cyclones identified at 500 or 300 hPa, with fewer cyclones identified but much larger mean intensities and radii.

b. Vertical structure of individual cyclones

Globally, 50.4% of cyclones identified from surface MSLP are tracked to 500 hPa when using a constant intensity threshold with height, including 52% in the Northern Hemisphere and 49% in the Southern Hemisphere, similar to the previously reported values of 52% for the Southern Hemisphere in Lim and Simmonds (2007). The proportion of cyclones that are vertically organized is smaller (42.4%) if vertical tracking is started at 500 hPa, which is unsurprising as the overall number of cyclones identified at 500 hPa is 33% higher than at the surface. Cyclones are most likely to be vertically organized in the extratropics, while shallow surface cyclones are more common in the subtropics (Fig. 3). Shallow surface cyclones are particularly common east of Japan and the United States, where the warm Kuroshio and Gulf Stream could help influence cyclogenesis (Hirata et al. 2015; Nelson and He 2012), as well as over continental Australia during the summer

months where weak heat lows are a common phenomenon (Lavender 2017).

As shown in Fig. 3, the Southern Hemisphere has more zonally consistent features than the Northern Hemisphere. Deep cyclones are more common at higher latitudes in both hemispheres and in both seasons, while a relatively high proportion of deep cyclones close to the equator during the local warm season may reflect the detection of some tropical cyclones. Deep cyclones are also relatively common in the Tasman Sea east of Australia as well as east of South America and in the poleward part of the North Atlantic and North Pacific storm tracks. Interestingly, however, a large proportion of cyclones identified from MSLP off the east coasts of the United States and Japan are shallow systems.

4. Australian east coast lows

A hot spot of cyclone activity can be observed in the Tasman Sea between southeastern Australia and New Zealand at all levels, especially during the cool season May–October, with cyclones over the Australian land-mass more common at higher levels (Fig. 2). This has been noted previously (Dowdy et al. 2013b), with cutoff cyclones known to move across southeastern Australia prior to developing an associated surface cyclone off the east coast (Mills et al. 2010). Upper-level cyclones in the Tasman Sea are also more likely to be deep than in most other areas of the globe at the same latitude (Fig. 3). This means that there is an annual average of 0.28 deep surface cyclones (deg. lat.)⁻² in the region 25°–40°S, 148°–160°E, compared to a global average of 0.22 cyclones (degrees latitude)⁻² at the same latitude.

The following sections focus on cyclones in the region 25°–40°S, 148°–160°E to allow a more detailed analysis, including exploring the impacts and localized environmental conditions. This region has been explored previously from both a surface and upper-level perspective in individual studies on cyclones [known as east coast lows (ECLs)]. However, here we examine conditions

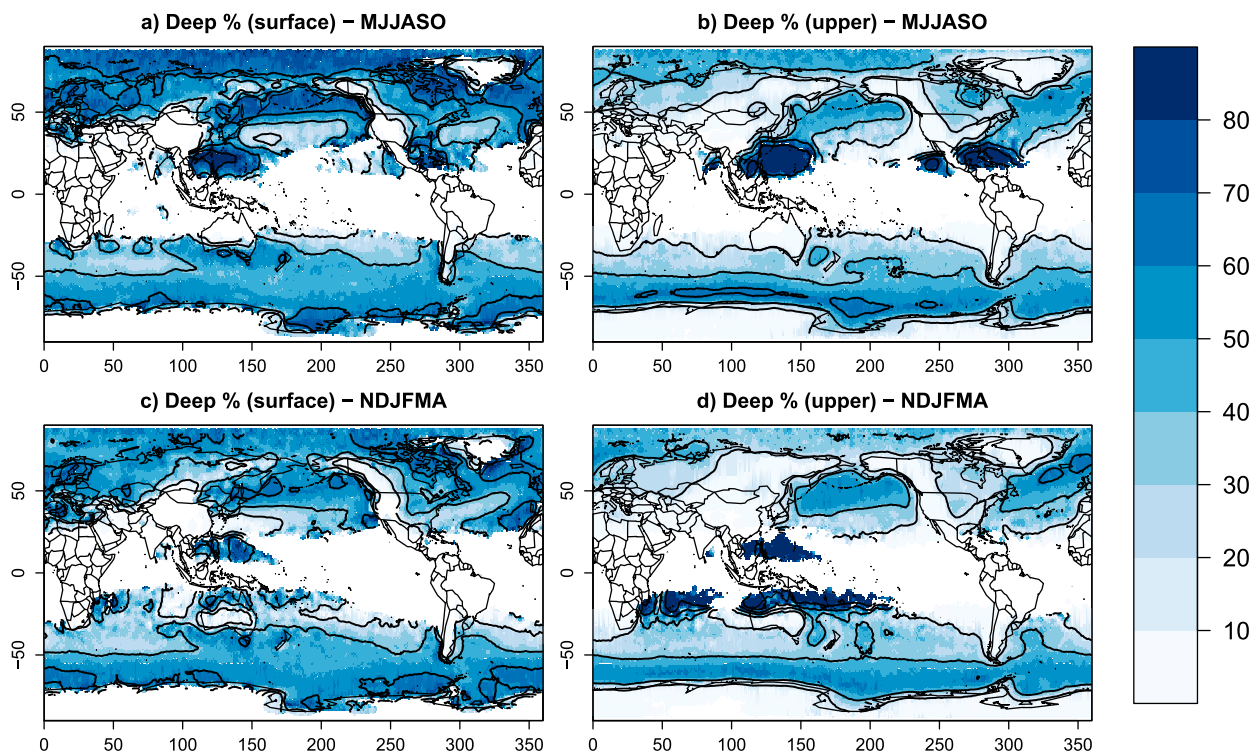


FIG. 3. Proportion of (left) surface and (right) 500-hPa cyclones in ERA-Interim between 1979 and 2016 that are vertically well organized during (top) May–October and (bottom) November–April. Solid contours are shown every 20% using a 5° averaging window.

throughout many levels of the troposphere in combination with each other, to investigate relationships between cyclone depth and associated severe weather conditions for this region.

As the number of cyclones in a given region varies with height, for the ECL region we vertically track cyclones using a height-varying intensity threshold that gives similar cyclone frequencies at each level, as explained in section 2 (Table 1). In this region there is strong agreement between cyclones identified at adjacent vertical levels, with 83% of surface cyclones identified up to 850 hPa and 83% of cyclones identified from 500-hPa GPH data also apparent at 600 hPa (Table 3). However, only a third of cyclones can be considered as deep cyclones, with a center identified at every level between MSLP and 500 hPa. When aggregated using the Hart (2003) phase space, shallow surface cyclones are found to be predominantly cold core, with cold core cyclones also forming more than 60% of cyclones that

are tracked to 200 or 300 hPa (Table 4). In comparison, the majority of midlevel cyclones have hybrid characteristics, with a shallow warm core and upper cold core.

When we look at ECLs as tracked events, more than half of ECLs identified initially from either MSLP or from 500-hPa geopotential height are part of events that can be tracked for over 48 h (Table 5). In both cases, longer cyclones are more likely to be vertically connected between MSLP and 500 hPa at some point while in the ECL region, while short-lived cyclones are more likely to be shallow. Similar results are seen if we separate events by their length of time within the ECL region: of systems that spend at least 24 h in the ECL region, only 7% of surface systems and 14% of upper systems are shallow, compared to more than 60% of systems only identified at a single instance.

Examining the different average seasonality observed at different vertical levels (Fig. 4), 64%–66% of midlevel and deep surface cyclones, and 73% of shallow upper

TABLE 3. Proportion of surface (or 500 hPa) cyclones in the ECL region that can be tracked vertically to at least a given level.

	MSLP	925 hPa	850 hPa	700 hPa	600 hPa	500 hPa	300 hPa	200 hPa
Surface cyclone	100%	87%	83%	66%	47%	31%	24%	10%
Upper cyclone	36%	42%	46%	62%	83%	100%		

TABLE 4. Proportion of cold core, warm core, and hybrid cyclones in the ECL regions using the Hart (2003) phase space, separated by the maximum vertical level to which the cyclone can be traced.

	All	MSLP	925 hPa	850 hPa	700 hPa	600 hPa	500 hPa	300 hPa	200 hPa
Cold core	55%	78%	74%	64%	40%	31%	50%	62%	67%
Hybrid core	42%	22%	25%	36%	60%	60%	39%	36%	33%
Warm core	3%	0%	1%	0%	1%	9%	11%	2%	1%

cyclones, occur between May and October. In comparison, shallow surface cyclones are most common during austral spring and early summer and least common during June. Upper cyclones are most likely to be shallow if they are located over the Australian continent, and shallow upper cyclones are less common over the Tasman Sea (Fig. 5). This is broadly similar to the conceptual ideas presented in Mills et al. (2010), who showed for several case studies that the upper-level cyclones frequently move eastward across southeast Australia prior to developing an associated surface low as they approach the Tasman Sea, under favorable conditions. In comparison, surface cyclones are most likely to be shallow near the coast, possibly suggesting a tendency to develop in coastal troughs or onshore easterly flow.

Compared to shallow surface cyclones, midlevel and deep surface cyclones also have higher intensities and longer durations, and are more likely to have closed circulation at MSLP in at least one instance (Table 6). They also have slightly slower movement speeds, and spend almost 5 times as long in the ECL region. While shallow upper cyclones have longer overall durations, they move significantly faster and spend less time in the ECL region. As with shallow surface cyclones, shallow upper cyclones are also less likely to have closed circulation and are less intense (i.e., have lower maximum Laplacians) than deep upper cyclones.

5. East coast low impacts

Table 6 shows that surface weather conditions are more severe for shallow surface lows than shallow upper lows. Surface wind speeds are strongest for deep cyclones,

whether the cyclone is initially tracked at the surface or at upper levels. The heaviest surface rain rates are also observed for surface cyclones that can be tracked vertically to the midtroposphere (midlevel and deep surface cyclones). This is consistent with previous case studies and examination of ECLs that have caused severe impacts on this region, as many of the most intense and damaging ECLs have had clear cyclones identified at multiple layers of the atmosphere, including the “Pasha Bulker” storm of June 2007 and the “swimming pool” storm of June 2016 (Dowdy et al. 2019). Thus 500-hPa vorticity has been previously found to be a good indicator of severe ECLs (Mills et al. 2010; Dowdy et al. 2013a). As the impacts of cyclones are often poorly correlated with their intensity at the surface (Pepler and Coutts-Smith 2013), it is important to understand how the vertical structure of cyclones can influence their impacts at the surface. The maximum rain rates for deep cyclones identified from upper levels are typically lower than for deep surface cyclones, which may relate to their asymmetrical vertical structure, discussed in section 6.

Compared to shallow surface cyclones, deep surface cyclones (that are identified up to 500 hPa) tend to have stronger intensities at MSLP as well as stronger mean wind speeds throughout the year (Table 6). At the time of maximum cyclone intensity (Fig. 6), the average wind speed within 500 km of the cyclone center is 11.7 m s^{-1} for deep surface cyclones compared to 9.6 m s^{-1} for shallow surface cyclones. In comparison, shallow upper cyclones have relatively weak surface wind speeds, although they may have stronger winds at upper levels than shallow surface cyclones.

Throughout the lifetime of the cyclone, deep and midlevel cyclones have higher maximum rain rates than shallow surface cyclones, both when calculated as the

TABLE 5. Event-based cyclone frequency and proportion of systems that are shallow or deep (as defined in Fig. 1), separated by event duration.

	Surface cyclones			Upper cyclones		
	<24 h	24–48 h	>48 h	<24 h	24–48 h	>48 h
Events per year	7.4	7.4	13.8	3.7	4.2	20.0
Hours in ECL region (per year)	10.3	18.2	50.6	4.7	7.7	62.1
Shallow %	52%	43%	24%	69%	75%	44%
Deep %	30%	28%	45%	25%	24%	48%

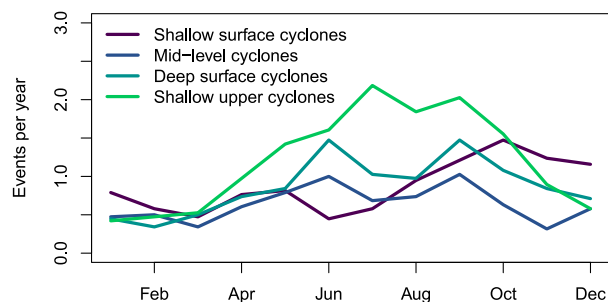


FIG. 4. Average number of cyclones per month in the ECL region, 1979–2016, stratified by their vertical structure.

heaviest point rainfall and when averaged over a 500-km radius around the cyclone (Table 6). In addition, as deep surface cyclones persist in the ECL region for longer (as shown in Table 6) than shallow surface cyclones, the average rainfall accumulation within 500 km of the cyclone center is more than double the average shallow surface cyclone. This highlights the importance of these deep systems for longer-duration events that can produce large accumulated totals in some regions, as can be important for streamflow and water availability in this region. When deep cyclones are first identified at 500 hPa rather than at the surface (deep upper cyclones), the peak

rain rates are lower than if identified at the surface, likely because the vertical tilt of the cyclone means some of the rainfall is displaced more than 500 km from the upper low. In comparison, shallow upper cyclones have much lower rain rates than any of the surface systems, with average total rainfall accumulations of just 2.8 mm.

Figure 7 shows the average MSLP, 500-hPa GPH, and TRMM rain rates for the time of peak rainfall around cyclones with different vertical structures. Compared to Fig. 6, the surface circulation at the time of maximum rain rate is slightly weaker and the upper-level trough or cyclone is located farther westward of the cyclone center. Heaviest rain rates are typically located to the south of the cyclone center for midlevel or deep surface cyclones, but are generally to the east of the cyclone center for shallow surface and shallow upper systems. While average rain rates are lower for shallow surface cyclones than deep systems, they produce consistently heavier rain rates than shallow upper cyclones, with a quarter of shallow surface cyclones producing heavy rainfall (Table 6). Rain rates are particularly low for shallow upper cyclones, with rain rates within 1000 km of cyclones typically below 1 mm h^{-1} , resulting in larger uncertainty as to the occurrence of rainfall in both satellite and reanalysis datasets.

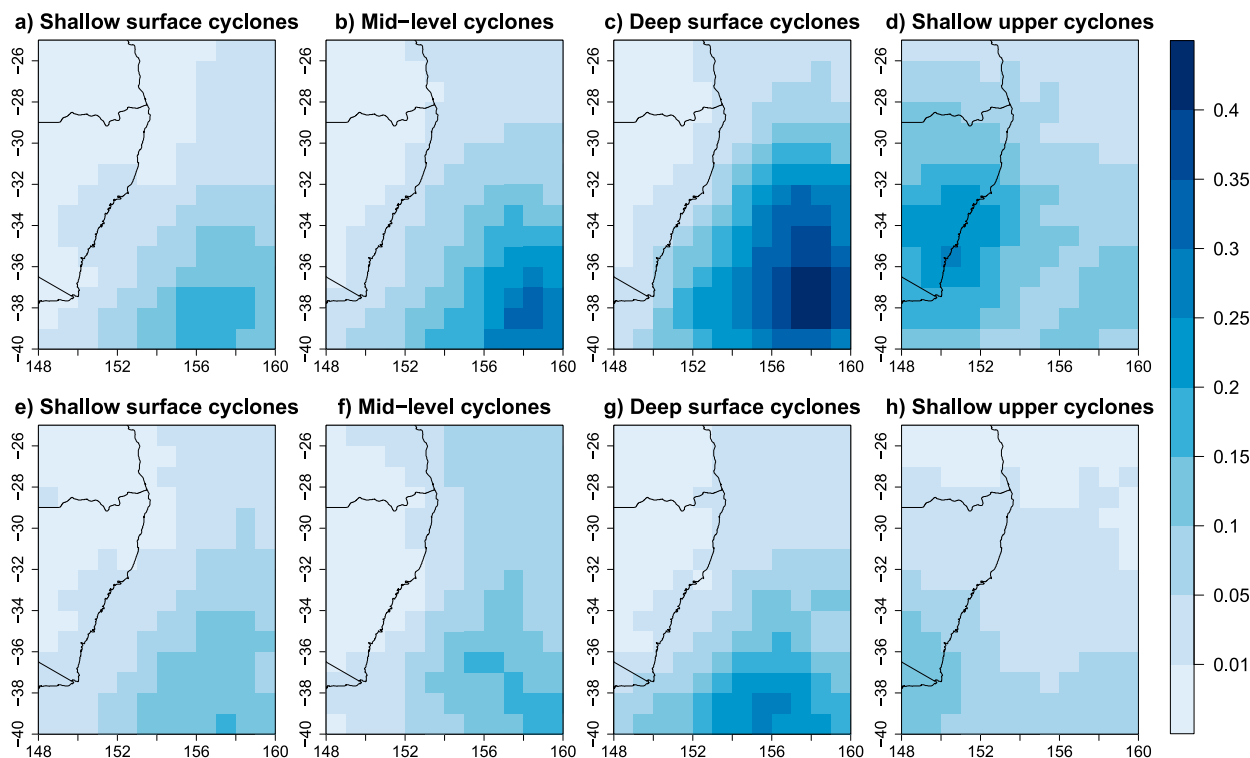


FIG. 5. Average frequency of cyclones [centers (degrees latitude) $^{-2}$, using a 2° smoothing radius] between 1979 and 2016 for (top) May–October and (bottom) November–April.

TABLE 6. Statistics for ECLs by their maximum depth, as defined in Fig. 1. Average and maximum wind/rain rates for each cyclone are calculated over a 500-km radius around the cyclone center. ECLs are considered to have heavy rainfall if the maximum rain rate is at least 25 mm h^{-1} or the maximum average rain rate is at least 1.5 mm h^{-1} . Statistical significance between the “shallow” and “deep” subsets is tested using a two-tailed two-sample Mann–Whitney U test for means and a two-tailed two-proportion Z test for proportions. In the “shallow” column for both surface and upper cyclones, statistical significance is indicated with italics for $p < 0.05$ and bold for $p < 0.001$.

	Shallow surface cyclones	Mid-level cyclones	Deep surface cyclones	Deep upper cyclones	Shallow upper cyclones
Events per year	10.5	7.7	10.4	11.4	14.5
Proportion in May–October	52%	63%	66%	64%	73%
Proportion ever closed	78%	88%	85%	86%	51%
Duration (h)	37.3	62.0	60.7	96.3	67.9
Time in ECL region (h)	3.8	13.4	15.3	15.6	5.4
Maximum Laplacian in ECL region	13.8	19.1	21.6	28.1	23.2
Speed in ECL region (km h^{-1})	27.8	26.6	24.4	37.8	51.7
Highest mean ERAI wind speed (m s^{-1})	9.6	10.8	11.7	11.2	9.2
Highest mean TRMM rain rate (mm h^{-1})	0.9	1.1	1.2	0.8	0.3
Maximum TRMM rain rate (mm h^{-1})	15.7	19.3	20.4	16.7	10.7
Mean total TRMM rainfall (mm)	7.4	14.6	17.4	10.9	2.8
Proportion with heavy rainfall	26%	36%	42%	16%	8%

The average circulation patterns for cyclones that produce heavy rainfall (Fig. 8) are broadly consistent with those shown for all cyclones, with heaviest rainfall to the south of the cyclone center for deep surface cyclones but farther east for shallow surface or shallow upper cyclones. To examine the environmental conditions associated with ECL rainfall, total column water vapor, CAPE, and lightning stroke counts are also

shown. ECLs with heavy rainfall are consistently associated with high values of total column water, particularly to the east and north of the cyclone, but also close to the cyclone center in the case of deep cyclones. However, they have very different patterns of convection depending on their vertical structure.

In the case of midlevel and deep surface cyclones, lightning is concentrated in the warm sector of the

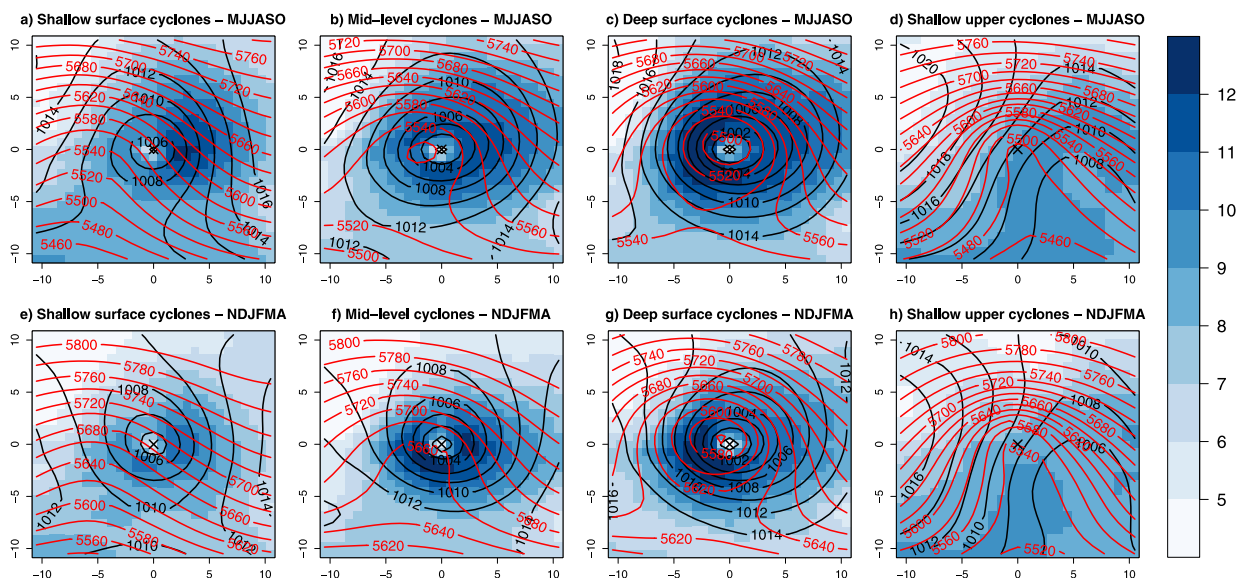


FIG. 6. 10-m wind speed (m s^{-1} ; shaded), MSLP (black), and 500-hPa geopotential height (red) at the instance of highest Laplacian within the ECL region based on cyclone vertical structure in (top) May–October and (bottom) November–April. Fields are composited for a radius of 10° around the cyclone center, with longitude shown on the x axis and latitude on the y axis.

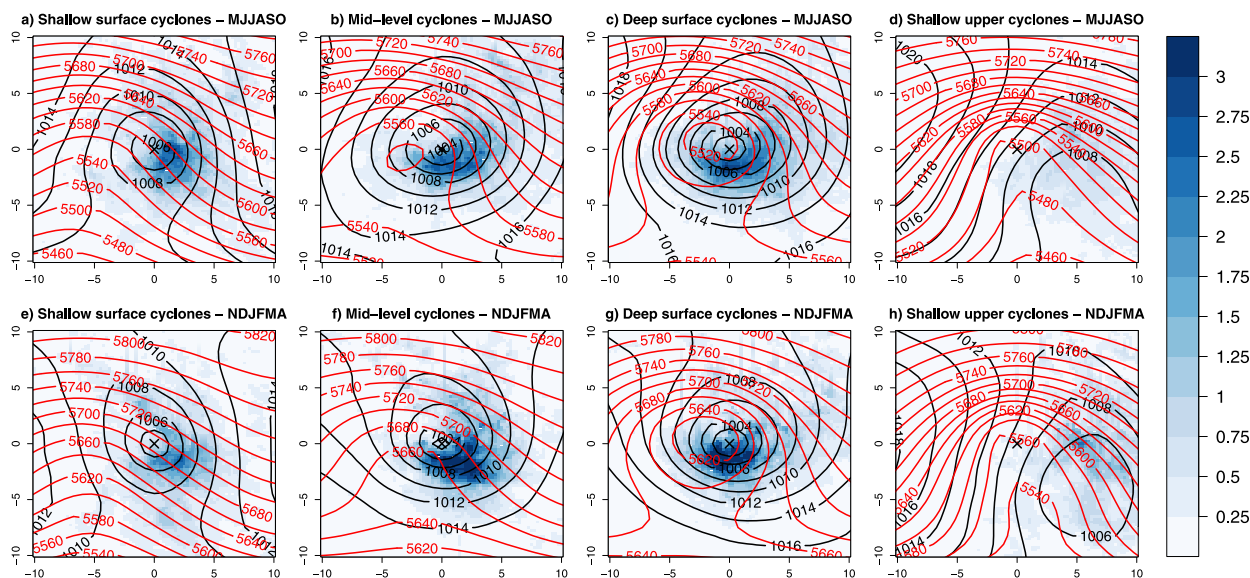


FIG. 7. TRMM rain rate (mm h^{-1} ; shaded), MSLP (black), and 500-hPa geopotential height (red) at the instance of highest average rainfall rates within the ECL region based on cyclone vertical structure in (top) May–October and (bottom) November–April.

cyclone, with 42% of low-rainfall and 53% of heavy-rainfall cyclones recording more than 100 lightning strokes at the time of peak rainfall intensity. Lightning plays a more important role in shallow cyclones: 72% of shallow surface cyclones with heavy rainfall recorded more than 100 lightning strikes, with an average of 1478 strikes, compared to 656 strikes for surface cyclones

without heavy rain ($p = 0.027$ using a two-tailed t test). Similarly, 80% of shallow upper cyclones with heavy rainfall recorded more than 100 lightning strikes, with an average of 1062 strikes compared to 264 strikes for cyclones without heavy rain ($p < 0.001$). This shows that convection plays an important role in the generation of rainfall from cyclones, consistent with previous studies

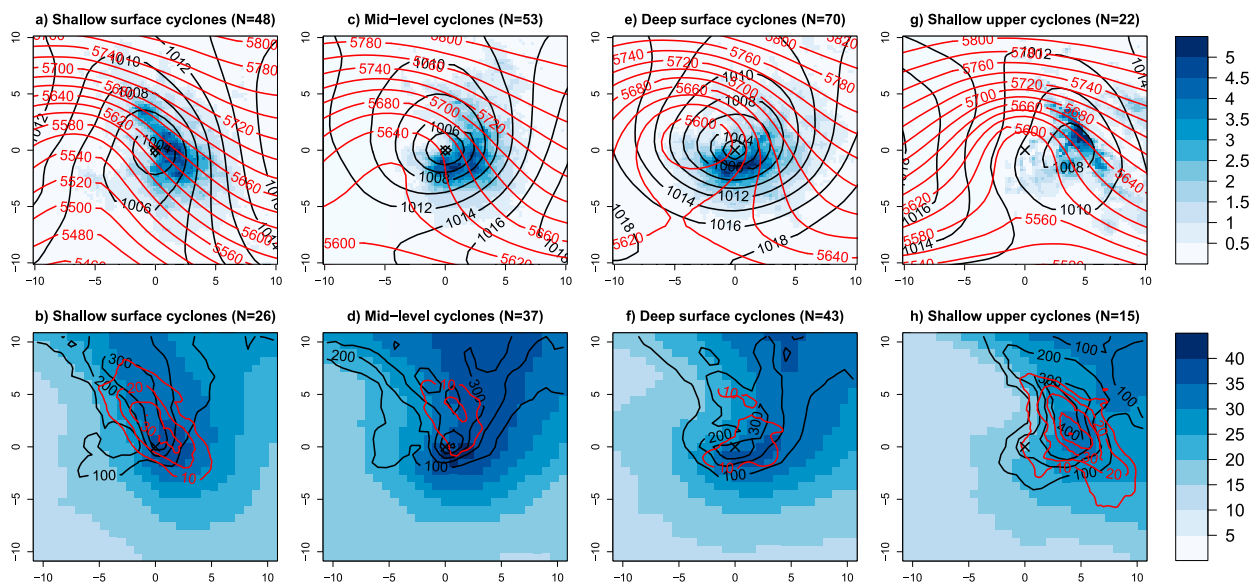


FIG. 8. Environmental characteristics at the instance of highest average rainfall rates, averaged for all cyclones that produced heavy rainfall within the ECL region, shown individually for cyclones of different vertical structures. (top) TRMM rain rate (mm h^{-1} ; shaded), MSLP (black), and 500-hPa geopotential height (red) and (bottom) ERA-Interim total column water (kg m^{-2} ; shaded) and most unstable CAPE (black; every 100 J kg^{-1}), and proportion of cyclones with lightning detected (red; every 10%, smoothed). The number of events in each group with rain data is listed in the top panel, with the bottom panels listing the number of events with lightning data available.

including in southeast Australia (Dowdy and Catto 2017; Chambers et al. 2015). Convection is particularly important in shallow cyclones that lack the deep vertical structure more commonly associated with extreme impacts.

6. East coast low development

Figure 9 shows how the circulation patterns and rain rates develop over time for ECLs relative to the time of maximum rain rates. The spatial and vertical structure of ECLs changes as the event develops. The heaviest rain rates typically occur as the cyclone is intensifying, as indicated by lower central pressures of the cyclone after the time of maximum rainfall intensity, consistent with previous studies of Pfahl and Sprenger (2016) and Booth et al. (2018a,b). The highest intensity rainfall occurs overwhelmingly while the cyclone is within the ECL region (90%), and frequently within the first 6 h for which the cyclone is identified (38%). The maximum Laplacian based on MSLP is reached on average 4.8 h after the time of peak rainfall intensity, increasing to 6.3 h later for cyclones that last for at least 24 h. Consistent with Mills et al. (2010), the upper cyclone is often located to the west or northwest of the surface cyclone during the period of maximum intensification and impacts (e.g., Fig. 6). The closest vertical alignment, based on the minimum horizontal distance between the MSLP and 500-hPa cyclone centers, occurs on average 10.8 h after the maximum rain rate.

Deep cyclones show a clear pattern of development, broadly consistent with studies elsewhere in the world (Pfahl and Sprenger 2016; Booth et al. 2018a). Whether we identify cyclones first at MSLP or at 500 hPa, at the time of peak rainfall the surface low is on average more than 200 km offset from the upper cyclone (Table 7). Where this distance is at least 250 km, such that relative locations are more robust, the upper low is located to the northwest of the surface low in most cases (70%). This result is similar to previous studies that have reported this general northwest tilt with height of cyclones in this region including Mills et al. (2010) and Lim and Simmonds (2007), corresponding to a baroclinic condition. Following the time of peak rainfall, the surface low continues to intensify and its radius increases, and the upper low moves eastward until the cyclone is vertically stacked (i.e., barotropic). The horizontal separation of the surface and upper cyclone at the time of peak rainfall may also explain the lower average rain rates for deep upper cyclones shown in Table 6, as the heaviest rain rates may be farther than 500 km from the center of the upper cyclone, or in some cases the upper cyclone may not be able to be tracked

vertically to the surface until after the time of peak rainfall.

While surface wind speeds remain high, average rain rates rapidly decrease from the peak of 1.2 mm h^{-1} to just 0.7 mm h^{-1} at the time the cyclone is vertically stacked (Table 7). This could be partially related to movement of the cyclone away from the vicinity of the warm East Australian Current, which contributes to increasing rainfall from ECLs near the coast (Pepler et al. 2016). Eddies and SST gradients within the East Australian Current have also been found to influence the location of lightning strikes and associated areas of high rainfall intensity (Chambers et al. 2014, 2015). The lightning stroke density also decreases over this period, while the total column water remains high, suggesting a potential weakening of the convectively driven rainfall during this time (i.e., associated thunderstorm activity as indicated by the observed lightning activity).

7. Discussion and conclusions

Cyclones are a common feature of the globe at all levels of the atmosphere. For a given intensity threshold, cyclones are most common at the surface and around the midtroposphere (500 hPa) and less common around 700 hPa. Globally, half of all cyclones identified at MSLP are vertically well organized and can be traced vertically to at least 500 hPa, with shallow surface cyclones most common in the subtropics.

On the east coast of Australia, 37% of ECLs identified from MSLP fields are deep surface cyclones that can be traced up to 500 hPa. Deep surface cyclones tend to be stronger, larger, and longer-lived than shallow surface cyclones, and are more likely to occur during the Southern Hemisphere cool season May–October. Deep surface cyclones also have higher maximum rain rates and wind speeds than shallow surface cyclones and spend longer in the ECL region, resulting in significantly larger total rainfall accumulations. However, shallow surface cyclones can sometimes produce heavy rainfall despite their lower intensities, which may potentially be related to associated thunderstorm activity [as discussed in Dowdy and Catto (2017)]. Consistent with Booth (2018a) and Pfahl and Sprenger (2016), the heaviest rainfall in both surface and deep cyclones typically occurs as the cyclone is intensifying, with deep cyclones producing highest rain rates while the upper low is located to the west of the surface cyclone (commonly associated with baroclinic conditions) and prior to the cyclone becoming vertically stacked (commonly associated with barotropic conditions).

As well as shallow surface cyclones, southeast Australia experiences a large number of shallow upper

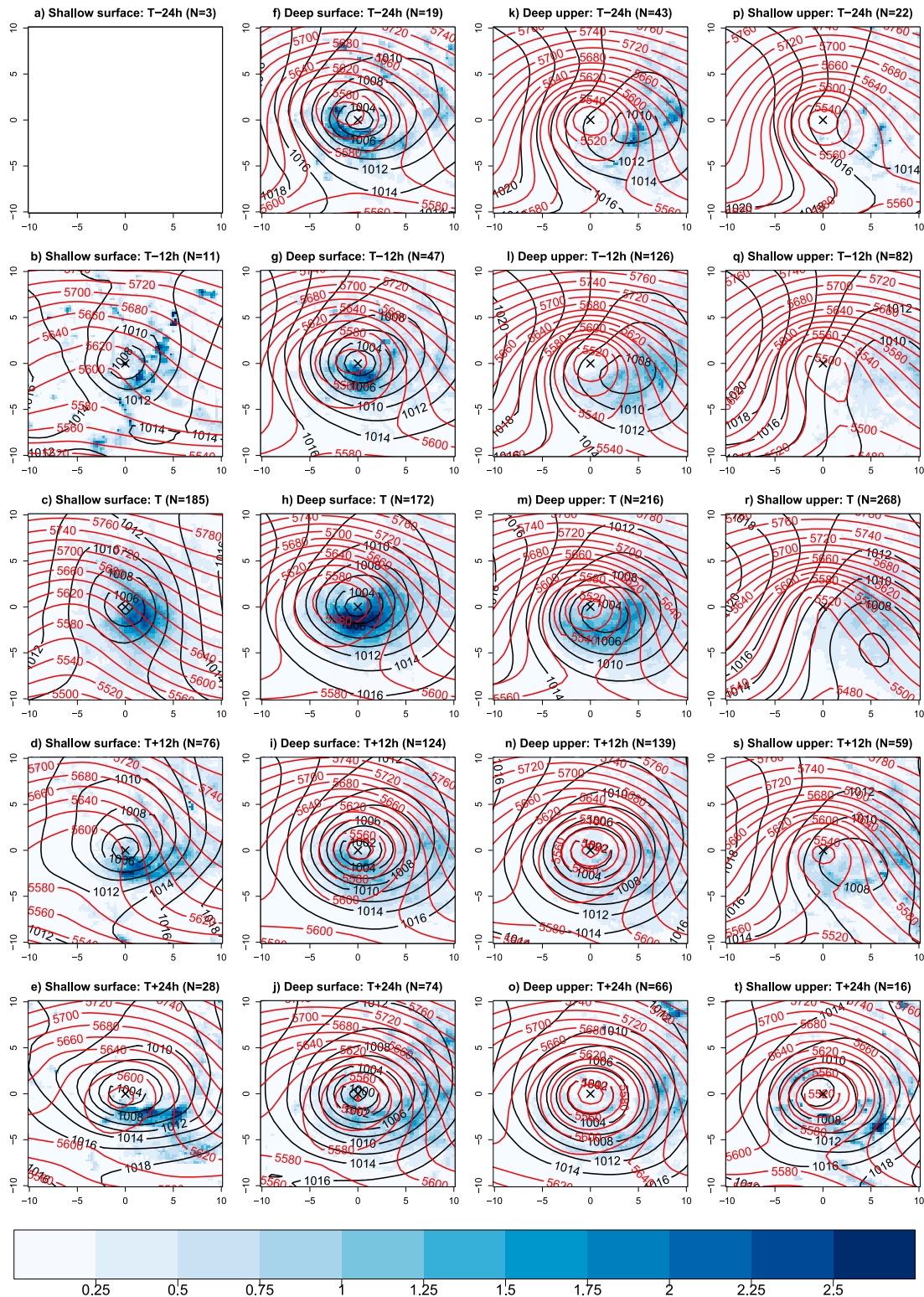


FIG. 9. TRMM rain rate (mm h^{-1} ; shaded), MSLP (black), and 500-hPa geopotential height (red) at the time of highest rainfall intensity as well as for times up to 24 h before and after the peak. Left panels are centered on the surface cyclone, for (left) surface-only and (center left) deep systems, while right panels are centered on the 500-hPa cyclone for (center right) deep and (right) upper-only systems. Note that the number of events included differs over time, as many cyclones persist for less than 24 h, particularly surface-only and upper-only systems. Composites are only shown where there are at least five systems to average.

TABLE 7. Selected statistics for deep surface cyclones relative to the time of highest rainfall intensity.

	$T - 24\text{ h}$	$T - 18\text{ h}$	$T - 12\text{ h}$	$T - 6\text{ h}$	T	$T + 6\text{ h}$	$T + 12\text{ h}$	$T + 18\text{ h}$	$T + 24\text{ h}$
% detected	11%	17%	27%	49%	100%	85%	71%	57%	42%
% in ECL region	26%	38%	46%	71%	100%	78%	68%	58%	48%
% deep	47%	45%	61%	55%	70%	74%	78%	63%	70%
Distance to 500 hPa cyclone (km)	178.4	146.5	188.4	195.7	223.4	191.7	152.8	135.3	127.6
Surface Laplacian	17.7	17.5	17.7	18.1	17.7	20.4	22.0	21.7	21.9
Upper Laplacian	30.9	30.4	30.1	28.7	28.3	28.6	28.1	27.7	25.4
Mean ERA-Interim wind speed (m s^{-1})	10.4	10.2	10.2	10.3	10.9	11.2	11.2	11.3	11.3
Mean TRMM rain rate (mm h^{-1})	0.6	0.5	0.7	0.7	1.2	0.8	0.6	0.5	0.5
Maximum TRMM rain rate (mm h^{-1})	11.4	10.4	12.2	14.7	18.2	14.1	12.1	11.6	10.1
Mean lightning frequency (counts)	28.8	47.5	522.4	466.9	580.3	218.3	170.1	119.8	41.3
Proportion ≥ 100 lightning strokes	13%	18%	35%	49%	45%	35%	37%	46%	17%
Mean total column water (kg m^{-3})	27.0	25.2	25.0	25.3	25.3	25.0	24.5	24.2	24.1

cyclones (i.e., without any surface cyclone development). These tend to be weaker and faster moving than deep upper cyclones (associated with a surface cyclone) and are particularly common over land areas. Shallow upper cyclones produce very little rainfall and have only weak surface winds, although they may have stronger winds at 500 hPa, so are of little relevance at the surface.

The results in this paper demonstrate that the vertical structure of cyclones plays a major role in their impacts at the surface, and should motivate a more three-dimensional approach to cyclone tracking and analysis in future studies. However, if cyclones are identified at only a single atmospheric level, surface cyclones are more likely to be associated with strong surface winds and heavy rainfall than upper cyclones. These findings clearly highlight a number of benefits from examining cyclones over multiple levels of the troposphere, including the importance of deep events for causing extreme weather events in this highly populated region of Australia. Future work will examine the factors influencing which upper cyclones develop a surface circulation and produce significant impacts at the surface.

Acknowledgments. This project is funded by the Earth Systems and Climate Change Hub of the Australian Government's National Environmental Science Program (NESP), and was assisted by resources from the Australian National Computational Infrastructure (NCI). The authors thank the Extreme Rainfall group of the ARC Centre of Excellence for Climate Extremes for valuable discussions that substantially improved this paper. The authors also thank Kevin Keay, Dragana Rajak, and three anonymous reviewers for their helpful comments on an earlier version of the manuscript, Marcus Thatcher for calculating the CAPE data used in this study, and Leone Cavicchia for calculating the Hart (2003) cyclone phase space diagnostics.

Data availability statement: The reanalysis and satellite datasets used in this paper are available via their

respective agencies. The cyclone tracking code is available from Ian Simmonds (<http://www.cycstats.org/tracks/cycstats4/>), and example tracking code is available at <https://github.com/apepler/cyclonettracking>. Derived cyclone datasets are available for research use by contacting the authors.

REFERENCES

- Allen, J. T., A. B. Pezza, and M. T. Black, 2010: Explosive cyclogenesis: A global climatology comparing multiple reanalyses. *J. Climate*, **23**, 6468–6484, <https://doi.org/10.1175/2010JCLI3437.1>.
- Booth, J. F., C. M. Naud, and J. Jeyaratnam, 2018a: Extratropical cyclone precipitation life cycles: A satellite-based analysis. *Geophys. Res. Lett.*, **45**, 8647–8654, <https://doi.org/10.1029/2018GL078977>.
- , —, and J. Willison, 2018b: Evaluation of extratropical cyclone precipitation in the North Atlantic basin: An analysis of ERA-Interim, WRF, and two CMIP5 models. *J. Climate*, **31**, 2345–2360, <https://doi.org/10.1175/JCLI-D-17-0308.1>.
- Callaghan, J., and P. Helman, 2008: Severe storms on the east coast of Australia, 1770–2008. Griffith Centre for Coastal Management, Griffith University, 240 pp.
- , and S. Power, 2014: Major coastal flooding in southeastern Australia, associated deaths and weather systems. *Aust. Meteor. Oceanogr. J.*, **64**, 183–213, <https://doi.org/10.22499/2.6403.002>.
- Catto, J. L., 2018: A new method to objectively classify extratropical cyclones for climate studies: Testing in the southwest Pacific region. *J. Climate*, **31**, 4683–4704, <https://doi.org/10.1175/JCLI-D-17-0746.1>.
- Cavicchia, L., A. Pepler, A. Dowdy, and K. Walsh, 2019: A physically based climatology of the occurrence and intensification of Australian east coast lows. *J. Climate*, **32**, 2823–2841, <https://doi.org/10.1175/JCLI-D-18-0549.1>.
- Chambers, C. R. S., G. B. Brassington, I. Simmonds, and K. Walsh, 2014: Precipitation changes due to the introduction of eddy-resolved sea surface temperatures into simulations of the “Pasha Bulker” Australian east coast low of June 2007. *Meteor. Atmos. Phys.*, **125**, 1–15, <https://doi.org/10.1007/s00703-014-0318-4>.
- , —, K. Walsh, and I. Simmonds, 2015: Sensitivity of the distribution of thunderstorms to sea surface temperatures in

- four Australian east coast lows. *Meteor. Atmos. Phys.*, **127**, 499–517, <https://doi.org/10.1007/s00703-015-0382-4>.
- Chang, E. K. M., S. Lee, and K. L. Swanson, 2002: Storm track dynamics. *J. Climate*, **15**, 2163–2183, [https://doi.org/10.1175/1520-0442\(2002\)015<02163:STD>2.0.CO;2](https://doi.org/10.1175/1520-0442(2002)015<02163:STD>2.0.CO;2).
- Dee, D. P., and Coauthors, 2011: The ERA-Interim reanalysis: Configuration and performance of the data assimilation system. *Quart. J. Roy. Meteor. Soc.*, **137**, 553–597, <https://doi.org/10.1002/qj.828>.
- Di Luca, A., J. P. Evans, A. Pepler, L. Alexander, and D. Argüeso, 2015: Resolution sensitivity of cyclone climatology over eastern Australia using six reanalysis products. *J. Climate*, **28**, 9530–9549, <https://doi.org/10.1175/JCLI-D-14-00645.1>.
- Dowdy, A. J., and J. L. Catto, 2017: Extreme weather caused by concurrent cyclone, front and thunderstorm occurrences. *Sci. Rep.*, **7**, 40359, <https://doi.org/10.1038/srep40359>.
- , G. A. Mills, and B. Timbal, 2011: *Large-Scale Indicators of Australian East Coast Lows and Associated Extreme Weather Events*. Australian Bureau of Meteorology, 104 pp.
- , —, and —, 2013a: Large-scale diagnostics of extratropical cyclogenesis in eastern Australia. *Int. J. Climatol.*, **33**, 2318–2327, <https://doi.org/10.1002/joc.3599>.
- , —, —, and Y. Wang, 2013b: Changes in the risk of extratropical cyclones in eastern Australia. *J. Climate*, **26**, 1403–1417, <https://doi.org/10.1175/JCLI-D-12-00192.1>.
- , —, —, and —, 2014: Fewer large waves projected for eastern Australia due to decreasing storminess. *Nat. Climate Change*, **4**, 283–286, <https://doi.org/10.1038/nclimate2142>.
- , and Coauthors, 2019: Review of Australian east coast low pressure systems and associated extremes. *Climate Dyn.*, **53**, 4887–4910, <https://doi.org/10.1007/s00382-019-04836-8>.
- ECMWF, 2009: ERA-Interim project. National Center for Atmospheric Research Computational and Information Systems Laboratory Research Data Archive, accessed 1 July 2018, <https://doi.org/10.5065/D6CR5RD9>.
- Evans, J. P., and I. Boyer-Souchet, 2012: Local sea surface temperatures add to extreme precipitation in northeast Australia during La Niña. *Geophys. Res. Lett.*, **39**, L10803, <https://doi.org/10.1029/2012GL052014>.
- Flaounas, E., S. Raveh-Rubin, H. Wernli, P. Drobinski, and S. Bastin, 2015: The dynamical structure of intense Mediterranean cyclones. *Climate Dyn.*, **44**, 2411–2427, <https://doi.org/10.1007/s00382-014-2330-2>.
- Fuenzalida, H. A., R. Sánchez, and R. D. Garreaud, 2005: A climatology of cutoff lows in the Southern Hemisphere. *J. Geophys. Res.*, **110**, D18101, <https://doi.org/10.1029/2005JD005934>.
- Graf, M. A., H. Wernli, and M. Sprenger, 2017: Objective classification of extratropical cyclogenesis. *Quart. J. Roy. Meteor. Soc.*, **143**, 1047–1061, <https://doi.org/10.1002/qj.2989>.
- Grieger, J., G. C. Leckebusch, M. G. Donat, M. Schuster, and U. Ulbrich, 2014: Southern Hemisphere winter cyclone activity under recent and future climate conditions in multi-model AOGCM simulations. *Int. J. Climatol.*, **34**, 3400–3416, <https://doi.org/10.1002/joc.3917>.
- Hart, R. E., 2003: A cyclone phase space derived from thermal wind and thermal asymmetry. *Mon. Wea. Rev.*, **131**, 585–616, [https://doi.org/10.1175/1520-0493\(2003\)131<0585:ACPSDF>2.0.CO;2](https://doi.org/10.1175/1520-0493(2003)131<0585:ACPSDF>2.0.CO;2).
- Hirata, H., R. Kawamura, M. Kato, and T. Shinoda, 2015: Influential role of moisture supply from the Kuroshio/Kuroshio Extension in the rapid development of an extratropical cyclone. *Mon. Wea. Rev.*, **143**, 4126–4144, <https://doi.org/10.1175/MWR-D-15-0016.1>.
- Hoskins, B. J., and K. I. Hodges, 2002: New perspectives on the Northern Hemisphere winter storm tracks. *J. Atmos. Sci.*, **59**, 1041–1061, [https://doi.org/10.1175/1520-0469\(2002\)059<1041:NPOTNH>2.0.CO;2](https://doi.org/10.1175/1520-0469(2002)059<1041:NPOTNH>2.0.CO;2).
- , and —, 2005: A new perspective on Southern Hemisphere storm tracks. *J. Climate*, **18**, 4108–4129, <https://doi.org/10.1175/JCLI3570.1>.
- Huffman, G. J., and Coauthors, 2007: The TRMM Multisatellite Precipitation Analysis (TMPA): Quasi-global, multiyear, combined-sensor precipitation estimates at fine scales. *J. Hydrometeorol.*, **8**, 38–55, <https://doi.org/10.1175/JHM560.1>.
- Hutchins, M. L., R. H. Holzworth, K. S. Virts, J. M. Wallace, and S. Heckman, 2013: Radiated VLF energy differences of land and oceanic lightning. *Geophys. Res. Lett.*, **40**, 2390–2394, <https://doi.org/10.1002/grl.50406>.
- Jones, D. A., and I. Simmonds, 1993: A climatology of Southern Hemisphere extratropical cyclones. *Climate Dyn.*, **9**, 131–145, <https://doi.org/10.1007/BF00209750>.
- Keable, M., I. Simmonds, and K. Keay, 2002: Distribution and temporal variability of 500 hPa cyclone characteristics in the Southern Hemisphere. *Int. J. Climatol.*, **22**, 131–150, <https://doi.org/10.1002/joc.728>.
- Kouroutzoglou, J., H. A. Flocas, K. Keay, I. Simmonds, and M. Hatzaki, 2012: On the vertical structure of Mediterranean explosive cyclones. *Theor. Appl. Climatol.*, **110**, 155–176, <https://doi.org/10.1007/s00704-012-0620-3>.
- , —, M. Hatzaki, K. Keay, I. Simmonds, and A. Mavroudis, 2015: On the dynamics of a case study of explosive cyclogenesis in the Mediterranean. *Meteor. Atmos. Phys.*, **127**, 49–73, <https://doi.org/10.1007/s00703-014-0357-x>.
- Lakkis, S. G., P. Canziani, A. Yuchechen, L. Rocamora, A. Caferri, K. Hodges, and A. O'Neill, 2019: A 4D feature-tracking algorithm: A multidimensional view of cyclone systems. *Quart. J. Roy. Meteor. Soc.*, **145**, 395–417, <https://doi.org/10.1002/qj.3436>.
- Lavender, S. L., 2017: A climatology of Australian heat low events. *Int. J. Climatol.*, **37**, 534–539, <https://doi.org/10.1002/joc.4692>.
- Leckebusch, G. C., and U. Ulbrich, 2004: On the relationship between cyclones and extreme windstorm events over Europe under climate change. *Global Planet. Change*, **44**, 181–193, <https://doi.org/10.1016/j.gloplacha.2004.06.011>.
- Lim, E. P., and I. Simmonds, 2007: Southern Hemisphere winter extratropical cyclone characteristics and vertical organization observed with the ERA-40 data in 1979–2001. *J. Climate*, **20**, 2675–2690, <https://doi.org/10.1175/JCLI4135.1>.
- Mesquita, M. D. S., D. E. Atkinson, I. Simmonds, K. Keay, and J. Gottschatck, 2009: New perspectives on the synoptic development of the severe October 1992 Nome storm. *Geophys. Res. Lett.*, **36**, L13808, <https://doi.org/10.1029/2009GL038824>.
- Mills, G. A., R. Webb, N. E. Davidson, J. Kepert, A. Seed, and D. Abbs, 2010: The Pasha Bulker east coast low of 8 June 2007. CAWCR Tech. Rep. 023, 62 pp., https://www.cawcr.gov.au/technical-reports/CTR_023.pdf.
- Murray, R. J., and I. Simmonds, 1991: A numerical scheme for tracking cyclone centres from digital data. Part I: Development and operation of the scheme. *Aust. Meteor. Mag.*, **39**, 155–166.
- Nelson, J., and R. He, 2012: Effect of the Gulf Stream on winter extratropical cyclone outbreaks. *Atmos. Sci. Lett.*, **13**, 311–316, <https://doi.org/10.1002/asl.400>.
- Neu, U., and Coauthors, 2013: Imilast: A community effort to intercompare extratropical cyclone detection and tracking algorithms. *Bull. Amer. Meteor. Soc.*, **94**, 529–547, <https://doi.org/10.1175/BAMS-D-11-00154.1>.

- Pepler, A. S., and C. S. Rakich, 2010: Extreme inflow events and synoptic forcing in Sydney catchments. *IOP Conf. Ser. Earth Environ. Sci.*, **11**, 012010, <https://doi.org/10.1088/1755-1315/11/1/012010>.
- , and A. Coutts-Smith, 2013: A new, objective, database of East Coast Lows. *Aust. Meteor. Oceanogr. J.*, **63**, 461–472, <https://doi.org/10.22499/2.6304.001>.
- , A. Di Luca, F. Ji, L. V. Alexander, J. P. Evans, and S. C. Sherwood, 2015: Impact of identification method on the inferred characteristics and variability of Australian east coast lows. *Mon. Wea. Rev.*, **143**, 864–877, <https://doi.org/10.1175/MWR-D-14-00188.1>.
- , L. V. Alexander, J. P. Evans, and S. C. Sherwood, 2016: The influence of local sea surface temperatures on Australian east coast cyclones. *J. Geophys. Res. Atmos.*, **121**, 13 352–13 363, <https://doi.org/10.1002/2016JD025495>.
- , A. Di Luca, and J. P. Evans, 2018: Independently assessing the representation of midlatitude cyclones in high-resolution reanalyses using satellite observed winds. *Int. J. Climatol.*, **38**, 1314–1327, <https://doi.org/10.1002/joc.5245>.
- Pezza, A. B., and T. Ambrizzi, 2003: Variability of Southern Hemisphere cyclone and anticyclone behavior: Further analysis. *J. Climate*, **16**, 1075–1083, [https://doi.org/10.1175/1520-0442\(2003\)016<1075:VOSHCA>2.0.CO;2](https://doi.org/10.1175/1520-0442(2003)016<1075:VOSHCA>2.0.CO;2).
- Pfahl, S., and H. Wernli, 2012: Quantifying the relevance of cyclones for precipitation extremes. *J. Climate*, **25**, 6770–6780, <https://doi.org/10.1175/JCLI-D-11-00705.1>.
- , and M. Sprenger, 2016: On the relationship between extratropical cyclone precipitation and intensity. *Geophys. Res. Lett.*, **43**, 1752–1758, <https://doi.org/10.1002/2016GL068018>.
- Pinto, J. G., T. Spanghel, U. Ulbrich, and P. Speth, 2005: Sensitivities of a cyclone detection and tracking algorithm: Individual tracks and climatology. *Meteor. Z.*, **14**, 823–838, <https://doi.org/10.1127/0941-2948/2005/0068>.
- Pook, M. J., J. S. Risbey, and P. C. McIntosh, 2014: A comparative synoptic climatology of cool-season rainfall in major grain-growing regions of southern Australia. *Theor. Appl. Climatol.*, **117**, 521–533, <https://doi.org/10.1007/s00704-013-1021-y>.
- Quinting, J. F., J. L. Catto, and M. J. Reeder, 2019: Synoptic climatology of hybrid cyclones in the Australian region. *Quart. J. Roy. Meteor. Soc.*, **145**, 288–302, <https://doi.org/10.1002/qj.3431>.
- Rudeva, I., and I. Simmonds, 2015: Variability and trends of global atmospheric frontal activity and links with large-scale modes of variability. *J. Climate*, **28**, 3311–3330, <https://doi.org/10.1175/JCLI-D-14-00458.1>.
- Simmonds, I., and K. Keay, 2000: Variability of Southern Hemisphere extratropical cyclone behavior, 1958–97. *J. Climate*, **13**, 550–561, [https://doi.org/10.1175/1520-0442\(2000\)013<0550:VOSHEC>2.0.CO;2](https://doi.org/10.1175/1520-0442(2000)013<0550:VOSHEC>2.0.CO;2).
- , and I. Rudeva, 2014: A comparison of tracking methods for extreme cyclones in the Arctic basin. *Tellus*, **66A**, 25252, <https://doi.org/10.3402/tellusa.V66.25252>.
- , R. J. Murray, and R. M. Leighton, 1999: A refinement of cyclone tracking methods with data from FROST. *Aust. Meteor. Mag.*, 35–49.
- Tilinina, N., S. K. Gulev, I. Rudeva, and P. Koltermann, 2013: Comparing cyclone life cycle characteristics and their inter-annual variability in different reanalyses. *J. Climate*, **26**, 6419–6438, <https://doi.org/10.1175/JCLI-D-12-00777.1>.
- TRMM, 2011: TRMM (TMPA) Rainfall Estimate L3 3 hour 0.25 degree \times 0.25 degree V7, Greenbelt, MD, Goddard Earth Sciences Data and Information Services Center (GES DISC), accessed 6 March 2018, <https://doi.org/10.5067/TRMM/TMPA/3H/7>.
- Virts, K. S., J. M. Wallace, M. L. Hutchins, and R. H. Holzworth, 2013: Highlights of a new ground-based, hourly global lightning climatology. *Bull. Amer. Meteor. Soc.*, **94**, 1381–1391, <https://doi.org/10.1175/BAMS-D-12-00082.1>.
- Wang, X. L., V. R. Swail, and F. W. Zwiers, 2006: Climatology and changes of extratropical cyclone activity: Comparison of ERA-40 with NCEP–NCAR reanalysis for 1958–2001. *J. Climate*, **19**, 3145–3166, <https://doi.org/10.1175/JCLI3781.1>.
- Wernli, H., and C. Schierz, 2006: Surface cyclones in the ERA-40 dataset (1958–2001). Part I: Novel identification method and global climatology. *J. Atmos. Sci.*, **63**, 2486–2507, <https://doi.org/10.1175/JAS3766.1>.
- Yanase, W., H. Niino, K. Hodges, and N. Kitabatake, 2014: Parameter spaces of environmental fields responsible for cyclone development from tropics to extratropics. *J. Climate*, **27**, 652–671, <https://doi.org/10.1175/JCLI-D-13-00153.1>.